ORIGINAL ARTICLE

Comparison study on dye degradation by PDA-SF/AgNPs-H$_2$O$_2$ and PDA-SF/AgNPs-PMS catalytic system

Aijing Li [a], Xinpeng Chen [a], Ping Yao [b], Jun Zhang [b], Tieling Xing [a,*], Guoqiang Chen [a]

[a] College of Textile and Clothing Engineering, Jiangsu Engineering Research Center of Textile Dyeing and Printing for Energy Conservation, Discharge Reduction and Cleaner Production (ERC), Soochow University, Suzhou 215123, China
[b] Suzhou Institute of Trade and Commerce, Suzhou 215009, China

Abstract In this work, polydopamine (PDA) was used to facilitate the reduction of silver nitrate (AgNO$_3$) to silver nanoparticles (AgNPs) and the simultaneous loading on waste silk fabrics (PDA-SF/AgNPs). The removal activity of the obtained composite PDA-SF/AgNPs on different dyes in the presence of hydrogen peroxide (H$_2$O$_2$) and potassium peroxymonosulfate (PMS) was compared. The effects of reaction temperature, H$_2$O$_2$/PMS dosage, dye concentration, composite dosage, electrolyte concentration and time in two catalyst systems on the dye removal were discussed. The results showed the dye removal of Telon Red A2R reached 81% and 95% in 30–50 min in PDA-SF/AgNPs-H$_2$O$_2$ and PDA-SF/AgNPs-PMS system, respectively. Quenching experiments demonstrated that $\cdot$OH, $\cdot$O$_2^-$ and SO$_4^-\cdot$ were produced during the degradation process, and the possible degradation pathway of Telon Red A2R were analyzed by HPLC-MS. In addition, the kinetic study indicated that the removal of dye followed quasi-second-order adsorption kinetics. These findings suggest that fabric-based composites have great potential and applications in catalysis and treatment of wastewater.

1. Introduction

In recent years, pollutants in the environment have increased as a result of rapid global industrialization and economic development, the increase of global population and the needs of daily production and life. Water is an important resource for human life, and almost all human activities generate wastewater (Babuponnusami and Muthukumar, 2014; Chaari et al., 2019; Y et al., 2018). The pollutants in these wastewaters, such as industrial dyes and toxic additives, seriously affect human health. Therefore, wastewater treatment has

* Corresponding author.
 E-mail address: xingtieling@suda.edu.cn (T. Xing).
Peer review under responsibility of King Saud University.

attracted a lot of attention (Mia et al., 2019; Zhang et al., 2014; Liu et al., 2021). Various technologies have been used to treat pollutants in water, including adsorption, biological treatment, photocatalytic treatment and advanced oxidation techniques, such as Fenton and Fenton-like reactions, which are usually used to degrade dyes in water (Brillas et al., 2009; Feng et al., 2021). For the oxidative treatment of wastewater, chemical, photochemical and electrochemical methods are commonly used to generate hydroxyl radicals in situ to oxidize organic pollutants in water to achieve the removal of pollutants. The $\cdot OH$ and $SO_4^-\cdot$ generated by H_2O_2 and potassium peroxymonosulfate (PMS) under certain conditions can oxidize organic matter indiscriminately and rapidly (Hong et al., 2022; Lai et al., 2020; Guan et al., 2020).

Nanosilver has a surface plasmon resonance effect (SPR), i.e. the surface valence electrons are collectively oscillated under the action of external fields such as light/heat, in which the nanosilver surface generates electron-hole pairs (e^- - h^+). And e^- and h^+ are involved in surface catalytic reactions with oxygen in water as well as water through electron transfer to produce superoxide anion radicals $O_2^-\cdot$ and $\cdot OH$, respectively, thus achieving the treatment of organic matter (Lu and Zhou, 2022; Rahn Kim et al., 2008; Udomkun et al., 2022). The synthesis of nanosilver mainly includes physical, chemical and biological methods. In recent years, due to the call for green chemistry and environment, as well as energy saving and emission reduction, the green preparation methods of nanosilver emerged. Researchers used lemon extract, biological flocculant and kapok fabric as reducing agents for the green synthesis of nanosilver particles (Eze et al., 2022; Kolya et al., 2019; Muthulakshmi et al., 2017; Divakar and Rao, 2017). Compared with other biomaterials, plant extracts are more widely available and convenient to use, making them suitable for large-scale preparation of nanomaterials.

Mussel-inspired polydopamine (PDA) has been proved to function as a universal adhesive layer on a variety of substrate surfaces and nanoparticles (Cui et al., 2018; Wang et al., 2019); this coating can form hydrogen electrostatic attraction, bond association, chelation and covalent bond with other matrix materials and possesses great potential in secondary functionalization. According to the formation mechanism of the PDA proposed in the existing literature, the joint action of covalent bond and non-covalent bond is one of the most comprehensive explanations (Guo et al., 2020; Xue et al., 2015; Wang et al., 2017). At the same time, some functional groups of PDA (such as amino and phenolic hydroxyl) can promote the reduction of metal ions. PDA is widely used as coating or binding layer in microbiology, catalysis and wastewater treatment due to its excellent properties (Cui et al., 2021; Tu et al., 2022). And in view of the serious global pollution situation and some advantages of nanosilver treatment of wastewater pollution, we speculate that nanosilver composites can be used as a research object to solve the problem of environmental pollution. However, Fenton reagent is easy to bring about secondary pollution, and nanosilver is difficult to be recycled. Loading nanosilver with certain substrate for wastewater treatment is a good solution. As a natural fibre with excellent properties and high added value in the textile field, silk has become a highly selective substrate for the preparation of functional textiles. Moreover, with the industrial use of silk, a large amount of waste silk is generated during the production process or after dyeing, and the modification of silk is imperative (Zhou and Zhang, 2022; Cao and Wang, 2017). Therefore, combining silver nanoparticles with waste silk into a new material is a feasible way. AgNPs are easily detached from the surface of silk fibers due to the poor adhesion between AgNPs and fibers. In recent years, in situ growth of AgNPs on the fiber surface has been developed as a simple and effective strategy to reduce silver ions (Ag^+) adsorbed on the fiber surface are directly reduced to form AgNPs by using eco-friendly biopolymers or natural plant extracts (e.g., catechol, polyphenols) as reducing agents (He et al., 2023; Hu et al., 2021; Chitichotpanya and Chitichotpanya, 2017). In addition, silk has better anti-mold properties than cotton, viscose and wool fibers (Zhang et al., 2019). It can effectively avoid the interference of mold microorganisms in the wastewater treatment process.

In this work, PDA was grafted onto the surface of waste silk by rapid oxidative polymerization, and then silver nanoparticles were reduced in situ on the waste silk fibers, which can effectively recover nanosilver and solve the waste problem of waste silk at the same time. Under two different catalyst systems, PDA-SF/AgNPs-H_2O_2 and PDA-SF/AgNPs-PMS, the toxic aromatic dyes can be removed. The surface morphology and chemical composition of the resulting composites was characterized by scanning electron microscopy (SEM), energy spectroscopy (EDS) and Fourier transform infrared spectroscopy (FT-IR). The effectiveness of the catalytic performance of this two catalyst systems was evaluated under the influence of dye concentration, temperature and electrolyte.

2. Materials and methods

2.1. Materials

Waste silk fabric (SF, 8.0 g/m^2, Jiangsu HuajiaGroup, China), dopamine hydrochloride (Yuanye Biotechnology Co. Ltd., Shanghai, China), 30% hydrogen peroxide (H_2O_2, Sinopharm Reagent), potassium peroxymonosulfate (PMS) were purchased from Shanghai Macklin Biochemical Technology Co. Ltd., China). Telon Red A2R was provided by Dystar (Shanghai) Trading Co., Ltd. Silver nitrate ($AgNO_3$), isopropyl alcohol (IPA), p-benzoquinone (BQ), methanol (MeOH), Rhodamine B (RhB), Direct dark brown ME (ME), Methylene blue (MB), sodium perborate tetrahydrate ($NaBO_3\cdot4H_2O$), tetrabutylammonium hydrogensulphate (TBAHS), acetonitrile and anhydrous ferric chloride ($FeCl_3$) were purchased from Shanghai Aladdin Biochemical Technology Co., Ltd., China. All the chemicals were of analytical reagent grade and used without further purification.

2.2. Preparation of PDA-SF

The waste silk was first washed with a mixture of Na_2CO_3 and soap flakes in water, then air dried under natural conditions. (2) g/L dopamine hydrochloride and 2.0 mmol/L $FeCl_3\cdot6H_2O$ were dispersed in 100 mL of deionized water. 1 g of waste silk fabric was added to the dopamine solution and placed in a shaking water bath for 10 min, followed by the addition of 9.0 mmol/L $NaBO_3\cdot4H_2O$. The final solution was stirred at 50 °C for 40 min. The obtained PDA-grafted waste silk fabric (PDA-SF) was rinsed and dried at 60 °C.

2.3. Preparation of PDA-SF/AgNPs

The PDA-SF prepared above was added to a conical flask containing 10.0 mmol/L (0.17 g) $AgNO_3$ in bath ratio of 1:100 and reacted at 35 °C for 6 h. The resulting PDA-SF-AgNPs were rinsed three times with deionized water and dried at 60 °C. The preparation process is shown in Fig. 1.

2.4. Material characterization

Fourier transform infrared (FTIR) spectroscopy was performed using a Nicolet-5700 FTIR spectrometer (Massachusetts, USA) on pristine and nanosilver-loaded SF. The samples to be tested were cut into powder and sampled with potassium bromide. The scan range was 600–4000 cm^{-1} and the scan time was 32 times. The surface morphology of all

Fig. 1 Preparation process of PDA-SF/AgNPs.

SF (before and after PDA grafting and nanosilver loading) was analyzed using a benchtop scanning electron microscope (Hitachi Ltd., Tokyo, Japan) at an accelerating voltage of 15 kV. Energy dispersive spectroscopy (EDS) was performed using a Bruckner axis EDS analyzer fitted with a SEM. In order to determine the surface enhanced Raman scattering properties of the PDA-SF-AgNPs, Raman testing of nanosilver modified silk was carried out. Various composites of appropriate size were taken and fixed on slides with double-sided tape and the Raman signals of the samples were tested by confocal Raman spectroscopy (LabRam HR Evolution, HORIBA Jobin Yvon S.A.S.,France) with an excitation wavelength of 532 nm. The crystal phase composition was also characterized by powder x-ray diffraction (XRD, Rigaku Smart Lab SE, Japan) using Cu Kα radiation (1.5418 Å). Narrow scan spectra of C 1 s, N 1 s, O 1 s and Ag 3d were fitted using x-ray photoelectron spectroscopy (XPS, Thermo Scientific K-Alpha, USA) as well as Avantage XPS software. The UV absorption spectra of Telon Red A2R solution was obtained at 529 nm on a UV–Vis spectrophotometer (TU1900, Beijing, China). The dye degradation products were determined by HPLC-MS (Agilent HPLC 1260, USA). The chromatographic separations were performed on hypersil columns, ODS (250×4.6 mm i.d.). Acetonitrile and 1 mmol/L aqueous tetrabutylammonium hydrogensulphate (TBAHS) (10:90, v/v) was used as eluent A against pure acetonitrile as eluent B. The velocity of flow remained 1 mL min^{-1}.

2.5. Adsorption experiments

The adsorption test of PDA-SF/AgNPs on the Telon Red A2R dye solution was carried out according to the following procedure. 0.1 g of PDA-SF/AgNPs was added to 50 mL of conical flasks with different dye concentrations under shaking conditions. The reaction was carried out at 40 °C for 40 min. The changes in the concentration of Telon Red A2R dye under different initial dye concentration were subsequently quantified by UV–Vis spectrum and standard curve of absorbance versus Telon Red A2R concentration.

2.6. Catalytic activity of PDA-SF/AgNPs

The catalytic properties of the synthesized PDA-SF/AgNPs composites were investigated using Telon Red A2R solution as a model contaminant. Under general conditions, 50 mL of dye solutions ($20 \sim 100$ mg/L) were treated with PDA-SF/AgNPs-H$_2$O$_2$/PMS ($0.1 \sim 10.0$ mmol/L) at specific temperatures ($30 \sim 80$ °C). The absorbance at the maximum absorption wavelength of the dye was determined by UV–Vis spectrophotometer and the corresponding dye residuals were calculated according to equation (1):

$$Removal\ rate = \frac{C0 - C}{C0} \times 100\% \qquad (1)$$

where C is the residual dye concentration at the specified time, and C_0 is the initial concentration of dye. Control experiments were carried out using H$_2$O$_2$/PMS, SF, PDA-SF and PDA-SF/AgNPs to investigate the adsorption and catalytic properties of two catalyst systems.

In addition, in order to determine the recoverability and reusability of the PDA-SF/AgNPs composites, the reproducibility of the composites under optimal conditions was investigated. The recovered composite was washed three times with ethanol and ultrapure water prior to the next catalytic test.

3. Results and discussion

3.1. Characterisation of PDA-SF/AgNPs composites

Polydopamine (PDA) was used to self-polymerize and graft onto the surface of the waste silk, and then Ag$^+$ was reduced to AgNPs by PDA as well as the reduction groups on the silk surface, such as amino and hydroxyl groups (Zhang et al., 2022), so as to realize the multilayer loading of nanosilver on the surface of silk. Changes in the surface morphology of the waste silk after different treatment are shown in Fig. 2. The pristine waste silk (SF) (Fig. 2a) shows a randomly overlapping network of fibers with a smooth surface. However, uniform clustered layers can be observed in PDA-SF (Fig. 2b), indicating that PDA is successfully grafted onto the fibre surface by rapid oxidative polymerization. After the addition of silver nitrate reaction, it can be found that there are a large number of nanosilver particles on the surface of PDA-SF/AgNPs (Fig. 2c), and it is obvious that the treated silk has an uneven clustered and mostly laminated surfaces. Therefore, it can be concluded that silver nanoparticles were successfully prepared and loaded onto the silk surface to form the required composite. Fig. 2d shows the PDA-SF/AgNPs after use. It can be seen that the prepared materials did not change significantly on the surface of silk fibers before and after use, and the AgNPs remained firmly loaded on the PDA-SF surface, indicating that the PDA-SF/AgNPs have good stability. TEM analysis was performed to accurately investigate whether Ag NPs were synthesized as well as the shape. In the TEM images, it can be seen that the nanosilver has spherical structure of
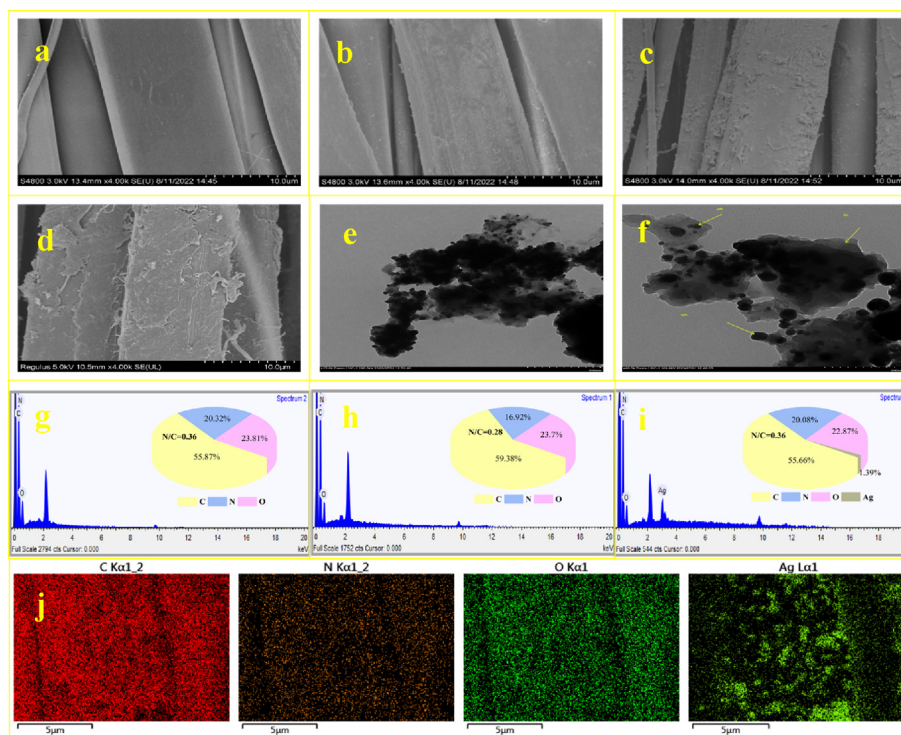
Fig. 2 SEM images and EDS of (a, g) SF, (b, h) PDA-SF, (c, i) PDA-SF/AgNPs and (d) PDA-SF/AgNPs after use, TEM images of Ag NPs at different magnifications (e, f) and (j) elemental mapping of PDA-SF/AgNPs.

particles (Farhadi et al., 2022; Jayarambabu et al., 2023). In addition, as shown in Fig. 2e-2f, TEM analysis revealed the presence of active substance PDA on the surface of AgNPs in the figure.

EDS analysis was carried out to further confirm the changes in the chemical composition of the fabric surface before and after treatment (Fig. 2g-2i). The surface elemental composition of the pristine and functionalized silk fabric is shown in pie charts. It can be concluded that the surface elemental N/C ratio of the treated fabric was significantly smaller than that of the pristine sample (Xie et al., 2021); proving that we have realized the modification of silk by PDA. After the addition of nanosilver loading, the elemental silver content ratio (1.39%) can be observed in the PDA-SF/AgNPs, indicating both the successful preparation of nanosilver and loading on the surface of the silk fibers. Accordingly, the EDS results proved that PDA was successfully modified the waste silk by self-polymerization and AgNPs were successfully prepared.

The chemical structure of SF, PDA-SF and PDA-SF/AgNPs were studied by FTIR spectroscopy. The characteristic absorption peak at $3276\,\mathrm{cm}^{-1}$ corresponds to the stretching vibration of –OH (An et al., 2020). The absorption peak observed at $1697\,\mathrm{cm}^{-1}$ can be attributed to the C = O stretching vibration (Wang et al., 2019), and the double absorption peak in the range $1650{-}1500\,\mathrm{cm}^{-1}$ corresponds to the bending vibration of the N–H bond. These peaks are visible in SF as well as in the prepared PDA-SF/AgNPs. It can be seen from Fig. 3a that the intensity of characteristic peaks on the SF surface decreased to different degrees after the silk was treated with PDA and loaded with Ag, mainly due to the SF surface was additionally covered. However, the characteristic peaks of Ag were not clearly observed in the FTIR spectra of

PDA-SF/AgNPs, which may be due to the relatively small amount of Ag. However, a decrease in the peaks of PDA-SF/AgNPs compared to PDA can be found, which laterally indicates the growth of AgNPs on the PDA-SF surface (Fig. 3a in the attached figure is a partial magnification of the wavelength $1750{-}500\,\mathrm{cm}^{-1}$). Fig. 3b shows the Raman pattern of the prepared composite. When the nanosilver was synthesized in situ on the PDA surface, the peaks of PDA can also be detected After the modification of silver nanoparticles, two distinctive characteristic peaks are observed at $1400\,\mathrm{cm}^{-1}$ and $1574\,\mathrm{cm}^{-1}$ (marked by * in the Fig. 3b), which correspond to the stretching and deformation vibrations of PDA catechol groups, respectively.

To further demonstrate the successful preparation of PDA-SF/AgNPs, the crystal structure and crystal orientation of the composites were characterized using XRD. Fig. 4a shows the XRD patterns of SF, PDA-SF and PDA-SF/AgNPs. Four characteristic peaks are observed at $2\theta = 37.47°$, $44.67°$, $64.94°$ and $77.69°$, corresponding to the (111), (200), (220) and (311) planes of face-centred cubic silver, respectively. The peak corresponding to the (111) plane is more intense than those in the other planes, indicating that the (111) plane is dominant. These XRD results showed that nanosilver was successfully formed by in situ reduction of PDA and loading of waste silk.

Fig. 4b shows the presence of Ag, C, N and O on the surface of the prepared PDA-SF/AgNPs composite. The narrow sweep spectrum of Ag 3d (Fig. 4c) shows that the two peaks of 367.3 eV and 373.3 eV are attributed to Ag $3d_{5/2}$ and Ag $3d_{3/2}$, respectively, which are typical binding energies for metallic Ag, indicating the loading of silver nanoparticles on the surface of PDA-SF. As shown in Fig. 4d, the peaks of C
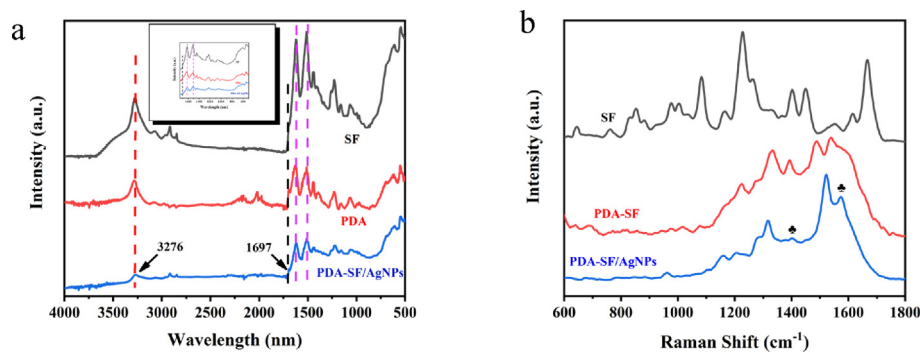
Fig. 3 (a) FTIR and (b) Raman spectrum of of SF, PDA-SF and PDA-SF/AgNPs.
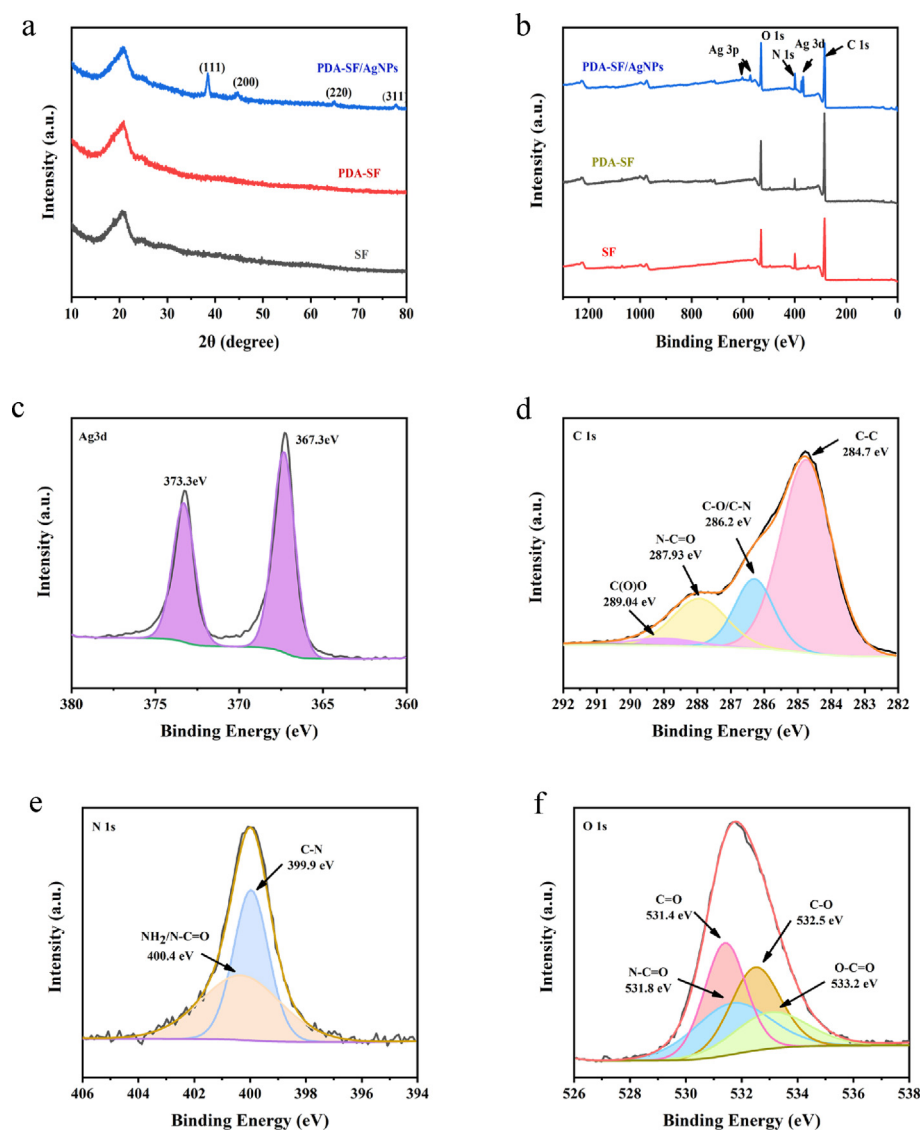

Fig. 4 XRD spectrum of of SF, PDA-SF and PDA-SF/AgNPs (a), Scanning XPS spectra of PDA-SF/AgNPs(b), high resolution XPS spectra of (c) Ag 3d, (d) C 1 s, (e) N 1 s and (f) O 1 s.

1 s for the PDA-SF/AgNPs are split into four signals including 284.7 eV (C–C), 286.2 eV (C-O/C–N), 287.93 eV (N–C = O) and 289.04 eV (C(O)O) (Li et al., 2022; Zhou et al., 2020; Zhang et al., 2022). The C 1 s spectra signal at 284.7 eV was ascribed to C–C which was derived from the benzene rings of PDA and the original silk. The peak at 286.2 eV belongs

to C–N derived from the amino group in the PDA side chains and the C–O in the phenolic hydroxyl groups of PDA. The peak at 287.93 eV belongs to N–C = O derived from to the original silk (Zangmeister et al., 2013). As shown in Fig. 4e; the peak at 399.9 eV was derived from imino groups in PDA (C–N). There was a significant peak at 400.4 eV (C–N = O), which was due to the crosslinking interaction between PDA and silk fibers (Wang et al., 2012; Duan et al., 2020). As for the O 1 s spectrum of PDA-SF/AgNPs (Fig. 4f), there were four types of O binding appeared at 533.2 eV (O–C = O), 532.5 eV (C-O), 531.8 eV (C–N = O), 531.4 eV (C = O), respectively, and the peak at 533.2 eV assigned to O–C = O group, which originated from the PDA (Duan et al., 2020). And the peak at 532.5 eV (C–O) may be influenced by the Ag metallisation process (He et al., 2023; Saidin et al., 2013). The XPS results clearly demonstrate the successful deposition of the PDA coating and the formation of silver nanoparticles, together with the preparation of the PDA-SF/AgNPs composites.

3.2. Catalytic oxidation performance

In order to investigate the catalytic oxidation performance of PDA-SF/AgNPs-H_2O_2 and PDA-SF/AgNPs-PMS systems for the dye, We explored at a Telon Red A2R concentration of 80 mg/L. We determined the reaction time to be 40 min and took 3 mL of liquid at 2 min intervals during the first 10 min and measured the absorption intensity at 529 nm. From Fig. 5, when the PDA-SF/AgNPs oxidation system was placed in dye solution, the absorption intensity at 529 nm decreased rapidly with time, indicating that the prepared PDA-SF/AgNPs composite has significantly enhanced catalytic oxidation activity for organic pollutants. Telon Red A2R was decolorized obviously in the first 10 min, and the removal rates were up to 76% and 92% in PDA-SF/AgNPs-H_2O_2 and PDA-SF/AgNPs-PMS system, respectively. In addition, since the decoloration of dyes may be affected by different factors, the type of dye adsorption was explored for this reason. The corresponding kinetic equation can be described as follows.

The pseudo-first-order kinetic equation:

$$\ln (Q_e - Q_t) = \ln Q_e - k_1 T \qquad (2)$$

Pseudo second-order kinetic equation:

$$t/Q_t = t/Q_e + 1/k_2 Q_e^2 \qquad (3)$$

where Q_e is the equilibrium adsorption capacity, Q_t is the adsorption capacity at time t in the presence of PDA-SF/AgNPs-H_2O_2 and PDA-SF/AgNPs-PMS, and k_1 and k_2 are the rate constants. As shown in Fig. 6, it is clear that the linear regression for the two catalytic systems both fit well to the pseudo-second-order kinetic model with rate constants of 0.9970 and 0.9984. The main reason for the enhanced catalytic activity of PDA-SF/AgNPs composites is the synergistic effect of waste silk fabric, PDA layer and silver nanoparticles.

3.2.1. Effect of temperature on decoloration
The effect of reaction temperature on the treatment of Telon Red A2R dye with PDA-SF/AgNPs-H_2O_2/PMS system was investigated. The reaction conditions were set as follows: C_0 (Telon Red A2R) = 80 mg/L, m (PDA-SF/AgNPs) = 0.10 g, t = 40 min, c (H_2O_2 /PMS) = 0.5 mmol/L, and T = 30 ∼ 80 °C, and the experimental results are shown in Fig. 7. It is evident from Fig. 6a that the removal rate of the reaction system changes little within the set temperature range. For PDA-SF/AgNPs-H_2O_2 system, compared with 30 °C, the dye removal rate increased more significantly at 40 °C, reaching 70.56%, and then further increased at 80 °C (75.42%). For PDA-SF/AgNPs-PMS system, Fig. 6b shows that the removal rate of the whole system reached the highest point at 50 °C (95.28%), followed by a slight decrease in dye removal rate with the increase of temperature, which may be due to a small amount of desorption of dye on the surface of the PDA-SF/AgNPs composite when the temperature is too high. In addition, high temperature will decompose PMS to some extent, affecting the action of $SO_4^-\cdot$ radicals, the possible action mechanism of free radicals is shown in 3.2.2. Considering energy saving, 40 °C and 50 °C were chosen as the optimal temperatures for dye decoloration in PDA-SF/AgNPs-H_2O_2 and PDA-SF/AgNPs-PMS system, respectively.

3.2.2. Effect of H_2O_2 and PMS concentrations on decoloration
The initial temperature of PDA-SF/AgNPs-H_2O_2 and PDA-SF/AgNPs-PMS systems was set at 40 °C and 50 °C, respectively, the initial concentration of dye was 80 mg/L, and the PDA-SF/AgNPs mass was 0.10 g. The effects of hydrogen peroxide (H_2O_2) and PMS concentration (0.1–10.0 mmol/L) on the decolorization of Talon red A2R dye were investigated. Fig. 8a shows the rate of dye removal in PDA-SF/AgNPs-H_2O_2 system increased when the H_2O_2 concentration was increased from 0.1 mmol/L to 0.5 mmol/L, and the dye removal rate reached the maximum (66.5%) at 40 min. With
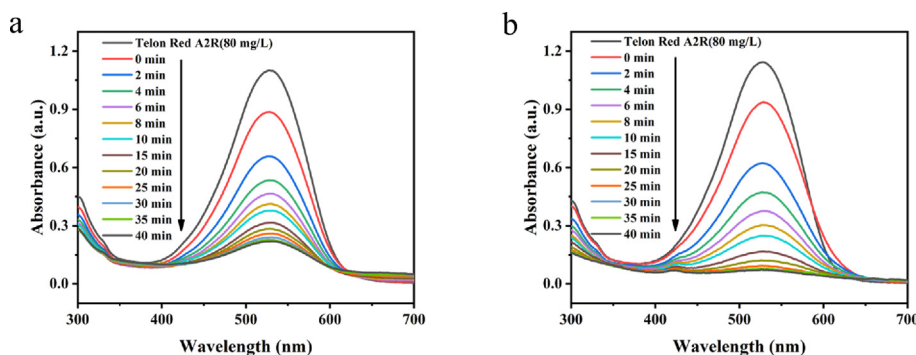

Fig. 5 Oxidative degradation on Telon Red A2R dye by (a) PDA-SF/AgNPs-H_2O_2 and (b) PDA-SF/AgNPs-PMS system.
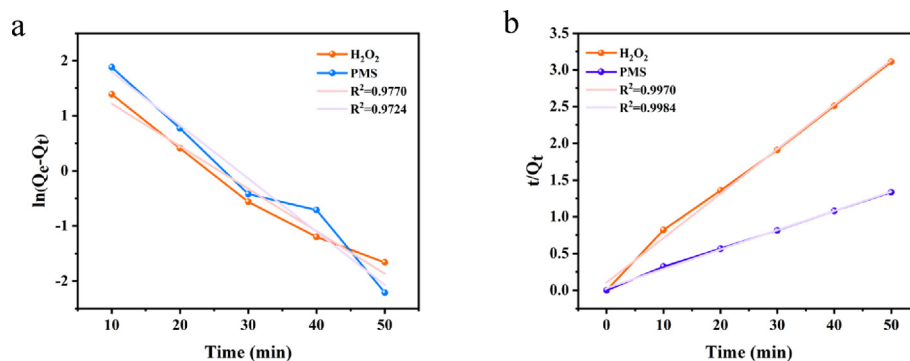
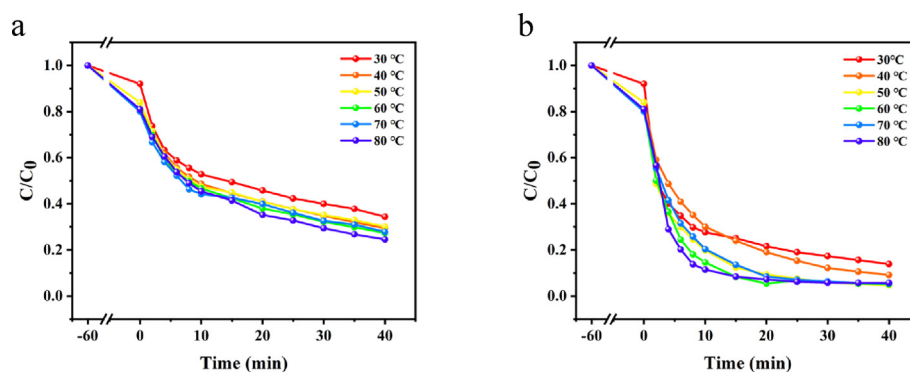**Fig. 6** The pseudo-first-order kinetic (a) and pseudo-second-order kinetic curves (b) and linear fits for the PDA-SF/AgNPs-H$_2$O$_2$/PMS systems.

Fig. 7 Effect of reaction temperature on decoloration of Telon Red A2R in PDA-SF/AgNPs-H$_2$O$_2$ (a) and PDA-SF/AgNPs-PMS systems (b).
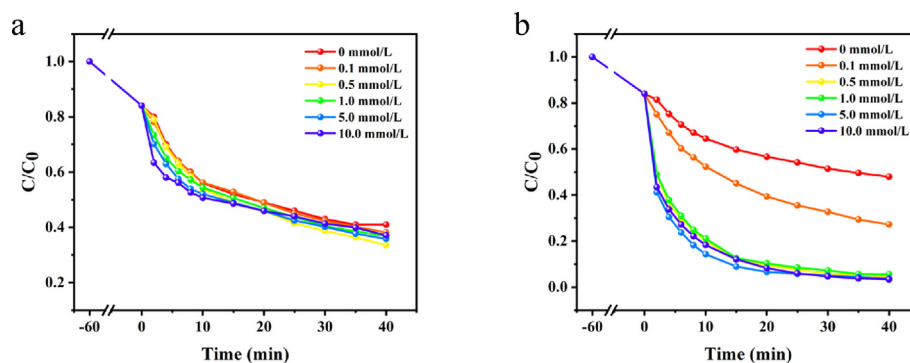

Fig. 8 Effect of H$_2$O$_2$ /PMS concentration on Telon Red A2R decoloration in PDA-SF/AgNPs-H$_2$O$_2$ (a) and PDA-SF/AgNPs-PMS system (b).
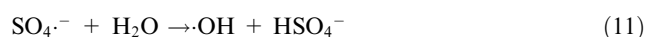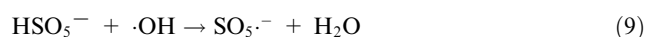
the increase of H$_2$O$_2$ concentration, AgNPs can be fully contacted with H$_2$O$_2$ to produce a large amount of ·OH radicals for dye decoloration. The relevant reactions are shown in the first two equations below. As the concentration of H$_2$O$_2$ further increases, there is a slight decrease in the removal rate of the dye. This may be due to the fact that the concentration of H$_2$O$_2$ is too high, the radicals produced have not yet reacted with the dye, and radicals are consumed with each other, which weakened the decoloration ability of the whole system. The reaction is shown in the following equations (Ershadi Afshar et al., 2018; Patil et al., 2018; Ai et al., 2014). The results show that when the dosage of PDA-SF/AgNPs was fixed, H$_2$O$_2$ concentration has a great influence on the decoloration ability of PDA-SF/AgNPs-H$_2$O$_2$ system.

$$AgNO_3 + PDA\text{-}SF \rightarrow PDA\text{-}SF/AgNPs \tag{4}$$

$$H_2O_2 \rightarrow 2\cdot OH \tag{5}$$

$$OH + H_2O_2 \rightarrow HO_2\cdot + H_2O \tag{6}$$

$$HO_2\cdot \rightarrow H^+ + \cdot O_2^- \tag{7}$$

$$HO_2\cdot + \cdot OH \rightarrow H_2O + O_2 \qquad (8)$$

At a PMS concentration of 0.5 mmol/L, the removal rate of PDA-SF/AgNPs-PMS system can reach 95% at 40 min (Fig. 8b). In the low concentration range of 0.1–0.5 mmol/L, the generation of free radicals was driven exclusively by the PMS concentration. With the increase of PMS concentration, a certain dose of PDA-SF/AgNPs can fully activate PMS, producing a large number of reactive free radicals for Telon Red A2R decoloration. The color removal rate of Telon Red A2R has no significant change (96%) when PMS concentration is greater than 0.5 mmol/L. This is because a certain amount of free radicals required for the composite is already sufficient for dye decoloration at a certain dye concentration. The relevant reaction mechanism is shown as follows (Liu et al., 2022; He et al., 2022; Li et al., 2022).

$$HSO_5^- + \cdot OH \rightarrow SO_5\cdot^- + H_2O \qquad (9)$$

$$2SO_5\cdot^- \rightarrow 2SO_4\cdot^- + O_2 \qquad (10)$$

$$SO_4\cdot^- + H_2O \rightarrow \cdot OH + HSO_4^- \qquad (11)$$

$$HSO_5^- \rightarrow H^+ + SO_5^{2-} \qquad (12)$$

$$3SO_5^{2-} + H_2O \rightarrow 2\cdot O_2^- + 3SO_4^{2-} + 2H^+ \qquad (13)$$

3.2.3. Effect of dosage of PDA-SF/AgNPs on decoloration

The dosage of PDA-SF/AgNPs composite is also an important factor affecting the color removal rate under certain dye concentration conditions, because AgNPs can act as a "bridge" to participate in dye decoloration. The influence of PDA-SF/AgNPs-H$_2$O$_2$ and PDA-SF/AgNPs-PMS system on the color removal rate under different PDA-SF/AgNPs dosage is shown in Fig. 9. From Fig. 9a, for PDA-SF/AgNPs-H$_2$O$_2$ system, a small dosage of PDA-SF/AgNPs (0.05 g) is not very effective for the decoloration of Telon Red A2R. When the dosage of PDA-SF/AgNPs was increased to 0.1 g, the removal rate of the dye could be increased by about 20%. This is due to the increase in the dosage of composite material, which improves the contact area between dyes and composite material, increases the generation of free radicals, and thus improves the color removal rate. When the dosage of PDA-SF/AgNPs was further increased to 0.2 g, there is another significant relative increase in the dye removal rate, and then there was no significant change in the final removal rate of the dye when the

dosage continued to increase. It can be judged that there was an optimum dosage of the composite (0.2 g) in the system when the dye removal rate basically reached the highest point and the PDA-SF/AgNPs composite was highly utilized. For PDA-SF/AgNPs-PMS system (Fig. 9b), the final color removal rate reaches 80% when the dosage of PDA-SF / AgNPs is low (0.05 g), while the final removal rate of the dye reaches 95% when the dosage of PDA-SF /AgNPs is increased to 0.1 g, and then the final removal rate of the dye does not change significantly when the dosage of the composite is increased again. This is due to the fact that the amount of the added composite is already sufficient to meet the demand of the dye, and a good synergistic reaction has been formed among the composite material, nanosilver and dye. Once the composite was added, the nanosilver could adsorb the dye tightly to the material, and nanosilver activated PMS to produce SO$_4$·radicals and immediately interacted with surrounding dyes to promote the decoloration of the dye.

3.2.4. Effect of electrolyte concentration on decoloration

In the practical production and life application, there are various electrolytes in the dye wastewater besides the dye itself, including NaCl, Na$_2$SO$_4$, Na$_2$CO$_3$, etc., which have an effect on the dye removal effect. For example, Cl$^-$ can capture hydroxyl radicals (Khattri and Singh, 2009). NaCl was used as a typical electrolyte and the influence of NaCl concentrations on the decoloration effect of dyes was investigated. Fig. 10 shows the presence of electrolytes has limited influence on the decoloration of Telon Red A2R, probably due to the complex structure of Telon Red A2R. The dye itself can react with the system, and the limited electrolyte has no significant impact on the internal and external reactions of the dye. This also indicates that the whole decoloration system is relatively stable and free from external influences.

3.2.5. Effect of reaction time on decoloration

The relevant reaction conditions were set as follows: C$_0$ (Telon Red A2R) = 80 mg/L, m (PDA-SF/AgNPs) = 0.20 g/0.10 g, T = 40 °C/50 °C, C (H$_2$O$_2$/PMS) = 0.5 mmol/L. The absorbance value of the dye solution was measured every 2 min in the first 10 min, and the experimental results are shown in Fig. 11. It can be seen that the first 10 min is the critical stage of the whole decolorization reaction. For PDA-SF/AgNPs-H$_2$O$_2$ system, the decoloration rate of Telon Red A2R could reach 81.45% at 50 min, and PDA-SF/AgNPs-PMS system could reach 94% at 30 min, achieving a good oxidative degra-
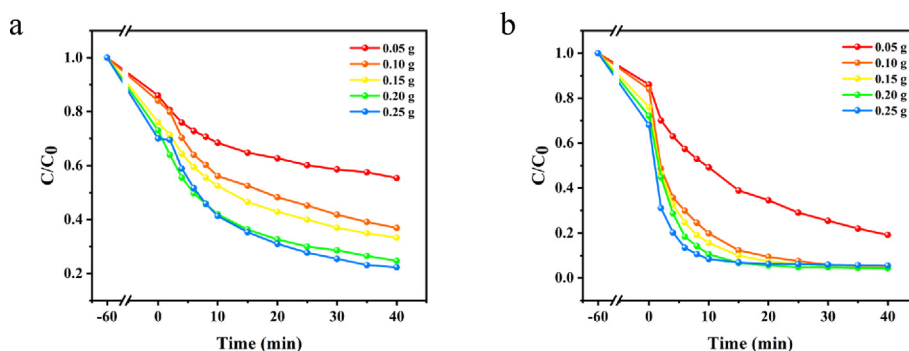

Fig. 9 Effect of PDA-SF/AgNPs dosage on A2R dye removal in PDA-SF/AgNPs-H$_2$O$_2$ (a) and PDA-SF/AgNPs-PMS systems (b).
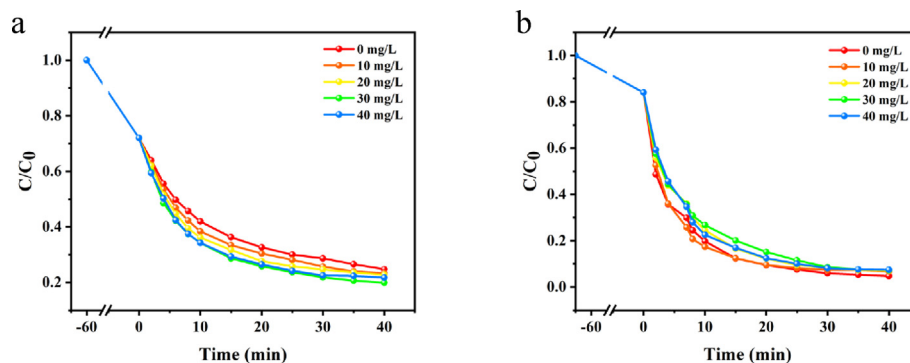
Fig. 10 Effect of electrolytes on Telon Red A2R degradation in PDA-SF/AgNPs-H$_2$O$_2$ (a) and PDA-SF/AgNPs-PMS systems (b).
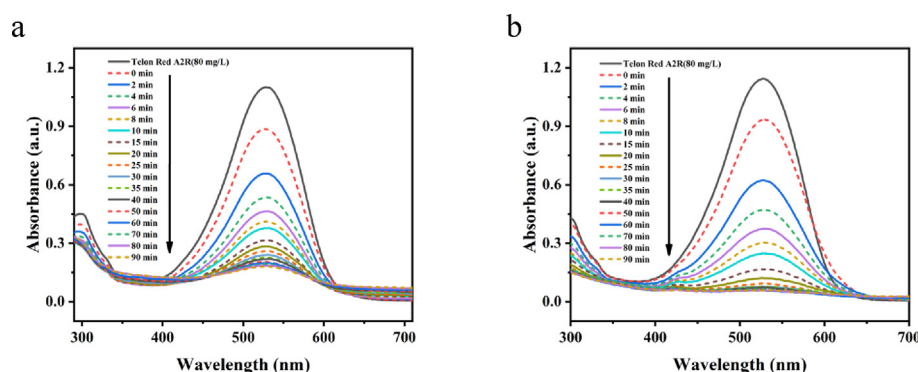

Fig. 11 Effect of reaction time on Telon Red A2R decoloration in PDA-SF/AgNPs-H$_2$O$_2$ (a) and PDA-SF/AgNPs-PMS system (b).

dation effect. By prolonging the reaction time, the residual dye concentration and the dye decoloration rate changed little, and the overall removal rate did not change significantly. It can be assumed that prolonging the reaction time will not significantly increase the dye removal rate. This is because under a certain dye concentration, the system consisting of added PDA-SF/AgNPs and oxidizing agent is already fully utilized. We hypothesize that by increasing the reaction time, a small amount of dyes adsorbed on the composite will be desorbed, thus affecting the oxidative decoloration of dyes. Therefore, for subsequent experiments, 50 min and 30 min of reaction time were selected for the dye decoloration by PDA-SF/AgNPs-H$_2$O$_2$ and PDA-SF/AgNPs-PMS systems, respectively.

3.2.6. Effect of different systems on decoloration

Fig. 12 shows the decoloration of Telon Red A2R for 40 min of reaction using differen systems. The removal rates of Telon Red A2R were 10.61%, 4.70%, 7.75%, 13.71%, 57.81%, 30.55%, 61.86%, 81.45% and 95.28% in the presence of H$_2$O$_2$, PMS, SF, PDA-SF, PDA-SF/AgNPs, AgNPs + H$_2$O$_2$, AgNPs + PMS and PDA-SF/AgNPs-H$_2$O$_2$/PMS systems, respectively. The above results indicated that the nanosilver particles deposited on the surface of PDA-SF fabric can significantly increase the oxidative decoloration rate of Telon Red A2R by the oxidant. This can be mainly attributed to adsorption of dyes by PDA-SF/AgNPs and electron transfer of nanosilver itself can generate under certain photothermal conditions, which enhances the free radical generation of the

oxidant (Wang et al., 2020), thus enabling more effective oxidization and decolorization of dyes.

3.3. Adsorption properties

The adsorption of Telon Red A2R dye molecules by catalyst is a prerequisite for the oxidative decoloration of dyes by oxidants H$_2$O$_2$ and PMS. Therefore, adsorption tests were carried out to better understand the oxidative decoloration of Telon Red A2R by oxidants using PDA-SF/AgNPs composite as catalyst. Fig. 13 shows the dye removal rates of different concentrations of Telon Red A2R solutions adsorbed by the prepared composites. When PDA-SF/AgNPs were added to the dye solution, there was a significant increase in the dye removal rate in the first 4 min. This was mainly attributed to the PDA layer of the composite and the action of the silver nanoparticles. PDA has abundant phenolic hydroxyl and benzene ring structures, resulting in electrostatic interactions and π-π stacking between the PDA layer and dye molecules. Due to electronic interactions, silver nanoparticles can also adsorb dye molecules (Cui et al., 2018; Jana et al., 1999).

3.4. Reusability of PDA-SF/AgNPs

The stability and recyclability of the composites are potentially essential factors in wastewater treatment applications in general. Fig. 14 shows the reusability of PDA-SF/AgNPs composites for oxidative decoloration of Telon Red A2R dye in the presence of oxidants in the system. After five cycles of reuse,
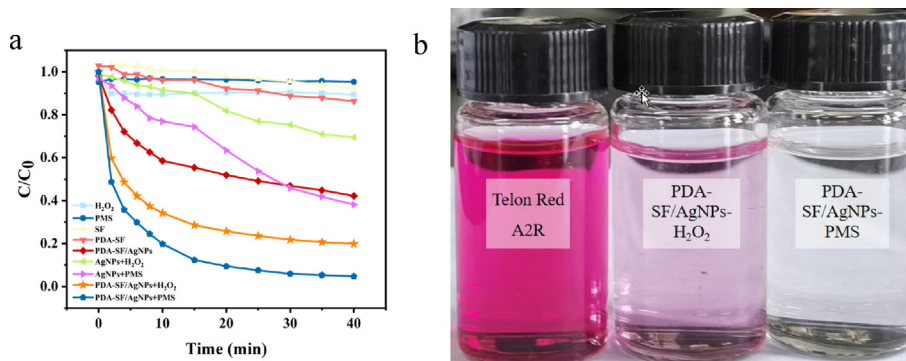
Fig. 12 Degradation rate curves of Telon Red A2R with different types of materials (a) and comparison before and after degradation (b).
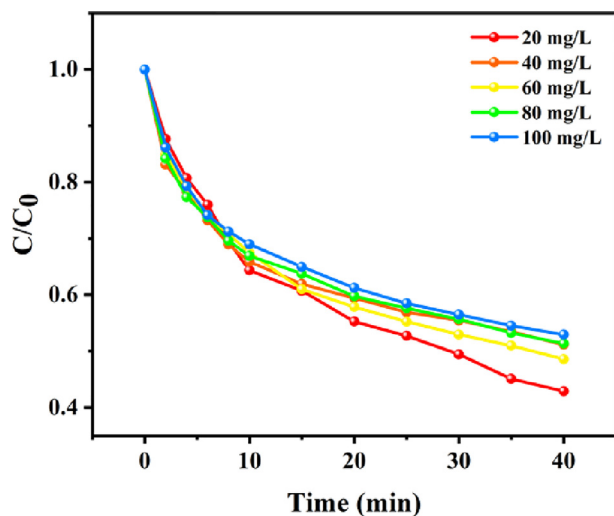

Fig. 13 Adsorption properties of PDA-SF/AgNPs composites.

although the catalytic performance of PDA-SF/AgNPs decreased slightly with the increase of the number of runs, the reused composites still showed high activity and could decompose nearly 70% of Telon Red A2R in five cycles (PDA-SF/AgNPs-H_2O_2) and remove 90% of Telon Red A2R in one hour in the fifth cycle (PDA-SF/AgNPs-PMS), indicating the high reusability and significant catalytic activity of the prepared composites of H_2O_2 and PMS oxidation systems.
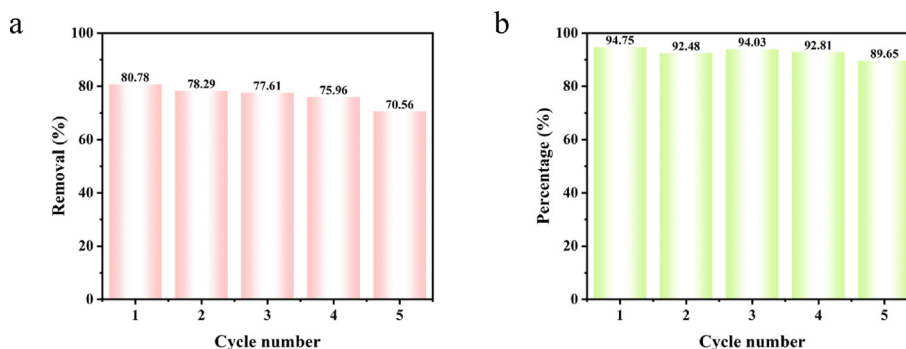
3.5. Potential mechanisms and pathways for dye degradation

In addition, in order to explore the reactive groups of PDA-SF/AgNPs-H_2O_2/PMS, isopropyl alcohol (IPA), p-benzoquinone (BQ) and methanol (MeOH) were used as scavengers of ·OH, ·O_2^- and ·OH/SO_4^-·. As shown in Fig. 15a, the degradation efficiency of Telon Red A2R varied less in the presence of BQ, with an inhibition rate of only 14% when the quenching reaction proceeded to 60 min, while the degradation efficiency decreased significantly after the addition of IPA (inhibition rates of about 30%). The results indicated that ·O_2^- and ·OH were the main active species. In particular, ·OH played a more important role than ·O_2^-, indicating that ·OH is the main active species in the degradation of Telon Red A2R solution. As shown in Fig. 15b, the degradation efficiency of Telon Red A2R varied less in the presence of BQ and IPA (inhibition rates of about 10% and 15%), while the degradation efficiency decreased significantly after the addition of MeOH (inhibition rates of about 30%). The results indicated that SO_4^-· was the main active specie. Therefore, it can be further verified that the content of OH· and SO_4^-· in the system has an important effect on the degradation of dyes.

Telon Red A2R has two sulfonic acid groups. Moreover, sulfonic acid being a strong electron withdrawing group, it should enhance dye decolorization. Zimmerman et al (Zimmermann et al., 1982; Patel et al., 2013) observed that such groups on phenyl ring of dye molecule also accelerated the decolorization process. Two such electronegative substituents (sulfo groups) existing on phenyl ring of Telon Red
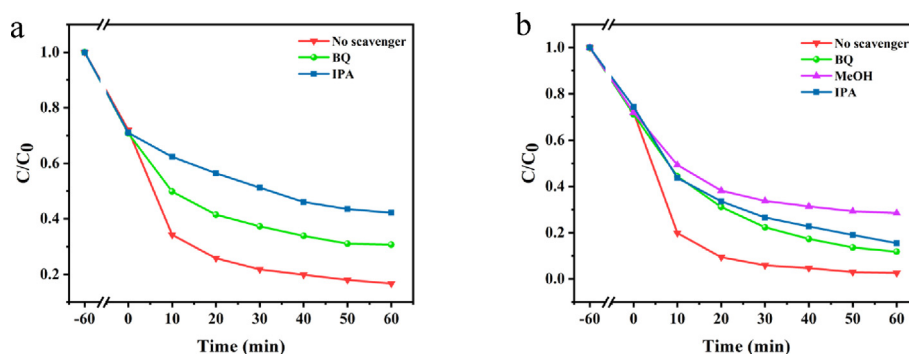

Fig. 14 Cyclic decoloration performance of (a) PDA-SF/AgNPs-H_2O_2 and (b) PDA-SF/AgNPs-PMS systems.

Fig. 15 Effects of scavengers on Telon Red A2R over (a) PDA-SF/AgNPs-H$_2$O$_2$ and (b) PDA-SF/AgNPs-PMS.
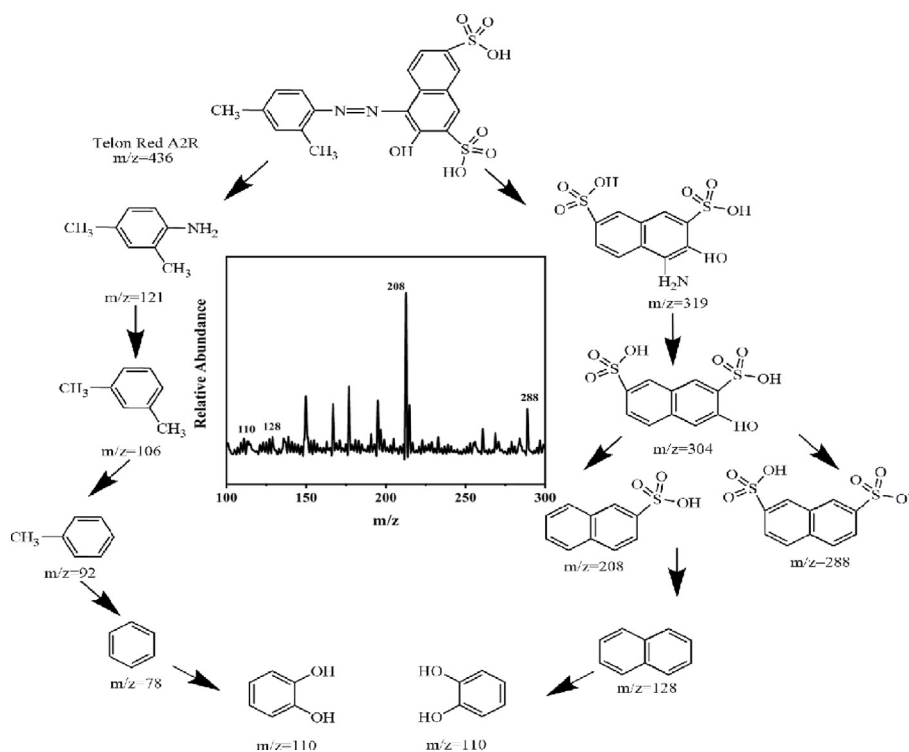

Fig. 16 Proposed degradation pathway of Telon Red A2R by PDA-SF/AgNPs-H$_2$O$_2$/PMS system.

A2R can accelerate decolorization, presumably because azo group render more accessible to free electron. Various mechanisms for azo dye degradation by microorganisms have been proposed. All these, generally follow two main routes as proposed by several studies: symmetrical or asymmetrical cleavage of azo bonds (López et al., 2004; Hong et al., 2007). Based on the identification of the intermediates, it is clear that Telon Red A2R has symmetric cleavage during the degradation process (Fig. 16). In consequence of the HPLC-MS analysis (inset in Fig. 16), we proposed four intermediary products of Telon Red A2R degradation at $m/z = 110, 128, 208$ and 288, respectively, indicating that Telon Red A2R was successfully degraded. The degradation pathway of Telon Red A2R by PDA-SF/AgNPs-H$_2$O$_2$/PMS system was also proposed.

The potential mechanisms for dye degradation by PDA-SF/AgNPs-H$_2$O$_2$/PMS system is put forward and shown in Fig. 17. There is a metal-like chelation between AgNPs and dyes (Sabouri et al., 2022), which enables dye molecules to tightly surround AgNPs. AgNPs itself can promote hydrogen peroxide and PMS to produce ·OH, O$_2^-$· and SO$_4^-$·, so that the generated free radicals can react with dyes around AgNPs, thus achieving the effect of dye oxidative degradation. Here the AgNPs act as a bridge for the reaction.

3.6. Decoloration of different dyes by PDA-SF/AgNPs-H$_2$O$_2$ and PDA-SF/AgNPs-PMS

In order to investigate the oxidative decoloration performance of the two systems PDA-SF/AgNPs-H$_2$O$_2$ and PDA-SF/AgNPs-PMS for different dyes, the final color removal rates of different dyes under the same conditions were also investigated in this work. The decoloration rates of Telon Red
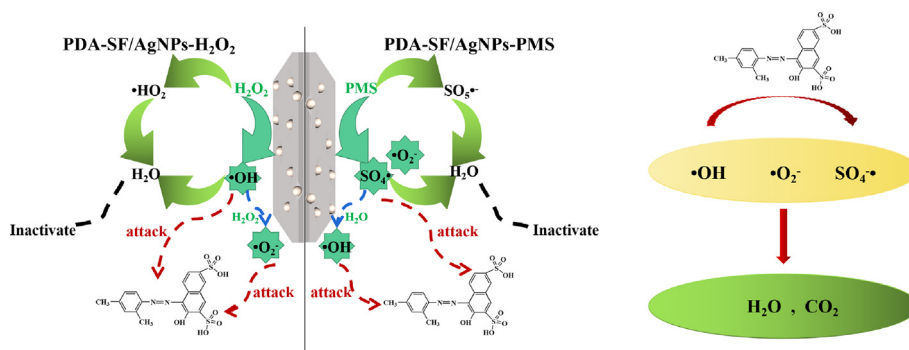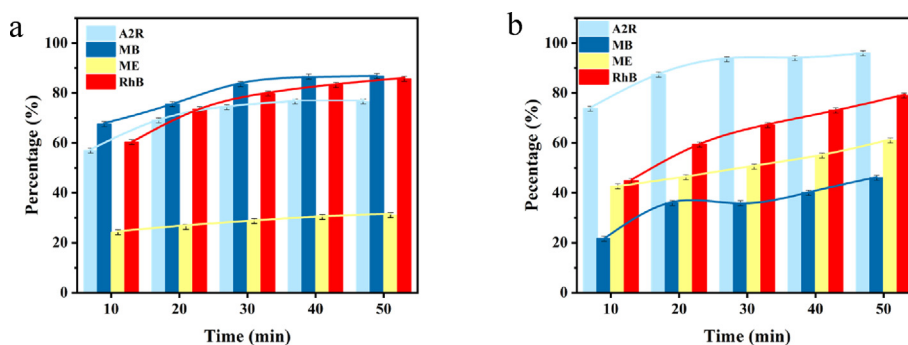
Fig. 17   Potential mechanisms for degradation.

Fig. 18   Decoloration performance of (a) PDA-SF/AgNPs-H$_2$O$_2$ and (b) PDA-SF/AgNPs-PMS systems for different dyes.

Table 1   Comparison on the dye degradation property of PDA-SF/AgNPs with materials in previous studies.

Material	Reducing agent	Reaction condition	Dye concentration	Time	Degradation percentage	Dye	Reference
AgNPs	Azadirachta indica	PMS	5×10^{-5} M	32 min	84%	AO10	(Nagar and Devra, 2019)
BiOBr/AgNW/CF	EG	Xenon light	10 mg/L	90 min	97%	RhB	(Wang et al., 2023)
C/PDA/Ag/AgCl	PDA	Xenon light	50 mg/L	180 min	95%	RB-19	(Ding et al., 2018)
Ag/AgCl/CeO$_2$ decorated cotton fabrics	ZnCl$_2$	Xenon light	20 mg/L	75 min	95.2%	MB	(Guan et al., 2020)
Ag-doped g-C$_3$N$_4$-TiO$_2$	–	Visible light	5 mg/L	150 min	94.5%	MO	(Li et al., 2023)
Ag-doped-ZnO/CaO	Caccinia macranthera	UV	10^{-5} M	100 min	90%	MB	(Sabouri et al., 2022)
Ca-ALG/MgO/Ag	NaBH$_4$	NaBH$_4$	50 mg/L	340 min	95%	Direct Red 83	(Albalwi, 2022)
Cu/Ag/Zn	Aqueous leaf	NaBH$_4$	0.04 mM	360 min	50.7%	Eosin yellow	(Kunwar et al., 2023)
Ag@GCN	Ocimum tenuiflorum	UV	10 mg/L	120 min	76% / 36%	RB XO	(Dahiya et al., 2023)
Ag/Fe$_3$O$_4$@h-BN	–	H$_2$O$_2$	10 mg/L	40 min	99.5%	MO MB RhB	(Xin et al., 2023)
PDA-SF/AgNPs	PDA	H$_2$O$_2$ PMS	80 mg/L	50 min 30 min	82% 95%	Telon Red A2R	this work

A2R, Rhodamine B (RhB), Direct dark brown ME (ME), Methylene blue (MB) dyes in PDA-SF/AgNPs-H$_2$O$_2$ and PDA-SF/AgNPs-PMS systems are shown in Fig. 18.

Fig. 18a-18b show the comparison of the degradation rates of the two systems for different dyes, and it can be seen that the two systems have different effects on different dyes, which may be due to the different damage occurring inside the structures of different dyes by OH· and SO$_4$·. It was shown that the PDA-SF/AgNPs + H$_2$O$_2$ and PDA-SF/AgNPs + PMS systems attacked the dyes with different intensities, resulting in

different degrees of dye bond breakage. In conclusion, these two systems have various effects on different dyes, with removal rates of up to 87% for MB (PDA-SF/AgNPs + H_2O_2) and 80% for RhB (PDA-SF/AgNPs + PMS), which are universal for the oxidative degradation of dyes of different structures. In addition, the effect of PDA-SF/AgNPs was comparable or even better than that of the reported similar type of catalytic composites (Table 1). Compared with some studies using chemical reducing agents, PDA used in this study has advantage of being green and environmentally friendly. In addition, the prepared PDA-SF/AgNPs have more desirable effect on the concentration up to 80 mg/L of Tenon red under the synergistic effect of H_2O_2 and PMS, and it can be found that the prepared PDA-SF/AgNPs have good recycling performance compared with nanomaterials based on the cyclic stability test and SEM images (Fig. 1d).

4. Conclusion

In this study, the loading of silver nanoparticles on polydopamine-modified waste silk was successfully achieved. It was shown that the nanosilver could be firmly loaded onto the silk surface with essentially no loss before and after use. There is a good synergistic effect among dyes, silver nanoparticles and oxidants, and the oxidanst can generate $\cdot O_2^-$, $\cdot OH$ and $SO_4 \cdot$ with the promotion of nanosilver to achieve the catalytic degradation of the dye. The results demonstrate that PDA-SF/AgNPs-H_2O_2 and PDA-SF/AgNPs-PMS systems have good reusability and stability. However, the two systems showed different degradation effects for different dyes. After different factors were explored, the two systems could finally obtain more than 82% and 95% degradation rates for Telon Red A2R, and the synthesized PDA-SF/AgNPs composite has a good application prospects for catalytic oxidation of dye pollutants in wastewater.

Declaration of Competing Interest

The authors declare that they have no known competing financial interests or personal relationships that could have appeared to influence the work reported in this paper.

Contributors

Aijing Li was responsible for experimental operation, paper writing and data processing; Xinpeng Chen was mainly responsible for data processing and experimental guidance; Ping Yao provided experimental guidance, some ideas and financial support; Jun Zhang provided experimental guidance; Tieling Xing provided experimental procedure guidance, paper guidance, paper revision and financial support and Guoqiang

Chen was mainly responsible for the guidance and revision of the thesis.

References

Ai, L., Zhang, C., Li, L., et al, 2014. Iron terephthalate metal–organic framework: revealing the effective activation of hydrogen peroxide for the degradation of organic dye under visible light irradiation[J]. Appl. Catal. B: Environ. 148, 191–200.

Albalwi, H.A., 2022. Synthesis and characterization of Ca-ALG/MgO/Ag nanocomposite beads for catalytic degradation of direct red dye [J]. Catalysts 13 (1), 78.

An, Y., Zheng, H., Yu, Z., et al, 2020. Functioned hollow glass microsphere as a self-floating adsorbent: rapid and high-efficient removal of anionic dye[J]. J. Hazard. Mater. 381, 120971.

Babuponnusami, A., Muthukumar, K., 2014. A review on Fenton and improvements to the Fenton process for wastewater treatment[J]. J. Environ. Chem. Eng. 2 (1), 557–572.

Brillas, E., Sirés, I., Oturan, M.A., 2009. Electro-Fenton process and related electrochemical technologies based on Fenton's reaction chemistry[J]. Chem. Rev. 109 (12), 6570–6631.

Cao, J., Wang, C., 2017. Multifunctional surface modification of silk fabric via graphene oxide repeatedly coating and chemical reduction method[J]. Appl. Surf. Sci. 405, 380–388.

Chaari, I., Fakhfakh, E., Medhioub, M., et al, 2019. Comparative study on adsorption of cationic and anionic dyes by smectite rich natural clays[J]. J. Mol. Struct. 1179, 672–677.

Chitichotpanya, P., Chitichotpanya, C., 2017. In vitro assessment of sericin-silver functionalized silk fabrics for enhanced UV protection and antibacterial properties using experimental design[J]. Coatings 7 (9), 145.

Cui, H., Li, Z., Wang, J., et al, 2021. Co-deposition integrating with interfacial polymerization to prepare PA/PDA/PVDF nanocomposite membrane and the application in the simulating RB5 dyeing wastewater treatment[J]. Desalin. Water Treat. 230, 359–371.

Cui, K., Yan, B., Xie, Y., et al, 2018. Regenerable urchin-like $Fe_3O_4@$ PDA-Ag hollow microspheres as catalyst and adsorbent for enhanced removal of organic dyes[J]. J. Hazard. Mater. 350, 66–75.

Dahiya, S., Sharma, A., Chaudhary, S., 2023. Synthesis of phytoextract-mediated Ag-doped graphitic carbon nitride (Ag@ GCN) for photocatalytic degradation of dyes[J]. Environ. Sci. Pollut. Res. 30 (10), 25650–25662.

Ding, K., Wang, W., Yu, D., et al, 2018. Facile formation of flexible Ag/AgCl/polydopamine/cotton fabric composite photocatalysts as an efficient visible-light photocatalysts[J]. Appl. Surf. Sci. 454, 101–111.

Divakar, T.E., Rao, Y.H., 2017. Biological synthesis of silver nano particles by using Bombax ceiba plant[J]. J. Pharm. Sci. 10 (1), 574–576.

Duan, M., Tang, Q., Wang, M., et al, 2020. Preparation of polydopamine-silk fibroin sponge and its dye molecular adsorption[J]. Water Sci. Technol. 82 (11), 2353–2365.

Ershadi Afshar, L., Chaibakhsh, N., Moradi-Shoeili, Z., 2018. Treatment of wastewater containing cytotoxic drugs by $CoFe_2O_4$ nanoparticles in Fenton/ozone oxidation process[J]. Sep. Sci. Technol. 53 (16), 2671–2682.

Eze, F.N., Ovatlarnporn, C., Nalinbenjapun, S., et al, 2022. Ultra-fast sustainable synthesis, optimization and characterization of guava phenolic extract functionalized nanosilver with enhanced biomimetic attributes[J]. Arab. J. Chem. 15, (10) 104167.

Farhadi, L., Mohtashami, M., Saeidi, J., et al, 2022. Green synthesis of chitosan-coated silver nanoparticle, characterization, antimicrobial activities, and cytotoxicity analysis in cancerous and normal cell lines[J]. J. Inorg. Organomet. Polym Mater. 32 (5), 1637–1649.

Feng, D., Lü, J., Guo, S., et al, 2021. Biochar enhanced the degradation of organic pollutants through a Fenton process using trace aqueous iron[J]. J. Environ. Chem. Eng. 9, (1) 104677.

Guan, Y.H., Chen, J., Chen, L.J., et al, 2020. Comparison of UV/ H$_2$O$_2$, UV/PMS, and UV/PDS in destruction of different reactivity compounds and formation of bromate and chlorate[J]. Front. Chem. 8, 581198.

Guan, X., Zhan, Y., Yang, L., et al, 2020. Durable and recyclable Ag/ AgCl/CeO 2 coated cotton fabrics with enhanced visible light photocatalytic performance for degradation of dyes[J]. Cellul. 27, 6383–6398.

Guo, Q., Chen, J., Wang, J., et al, 2020. Recent progress in synthesis and application of mussel-inspired adhesives[J]. Nanoscale 12 (3), 1307–1324.

He, B., Song, L., Zhao, Z., et al, 2022. CuFe$_2$O$_4$/CuO magnetic nanocomposite activates PMS to remove ciprofloxacin: Ecotoxicity and DFT calculation[J]. Chem. Eng. J. 446, 137183.

He, X.M., Zhu, T., Mao, H.Y., et al, 2023. Chitin whisker/dopamine enhancing in-situ generation of silver nanoparticles for fabricating functional silk fabrics[J]. Fibers Polym. 24 (5), 1649–1660.

Hong, Z., Cai, X., Zhang, W., et al, 2022. Construction of a FeCu/ ceramic composite with surface electric field and far-infrared properties for effective photo-Fenton catalytic degradation of the wastewater generated from H$_2$O$_2$ production[J]. J. Environ. Chem. Eng. 10, (3) 107687.

Hong, Y., Guo, J., Xu, Z., et al, 2007. Reduction and partial degradation mechanisms of naphthylaminesulfonic azo dye amaranth by Shewanella decolorationis S12[J]. Appl. Microbiol. Biotechnol. 75, 647–654.

Hu, Q., Zhou, Z., Gao, L., et al, 2021. Green synthesis of AgNP-decorated poly (dopamine) microcapsules for antibacterial applications[J]. Chemistry Select 6 (37), 10054–10058.

Jana, N.R., Sau, T.K., Pal, T., 1999. Growing small silver particle as redox catalyst[J]. J. Phys. Chem. B 103 (1), 115–121.

Jayarambabu, N., Velupla, S., Akshaykranth, A., et al, 2023. Bambusa arundinacea leaves extract-derived AgNPs: Evaluation of the photocatalytic, antioxidant, antibacterial, and anticancer activities [J]. Appl. Phys. A 129 (1), 13.

Khattri, S.D., Singh, M.K., 2009. Removal of malachite green from dye wastewater using neem sawdust by adsorption[J]. J. Hazard. Mater. 167 (1–3), 1089–1094.

Kolya, H., Kuila, T., Kim, N.H., et al, 2019. Bioinspired silver nanoparticles/reduced graphene oxide nanocomposites for catalytic reduction of 4-nitrophenol, organic dyes and act as energy storage electrode material[J]. Compos. B Eng. 173, 106924.

Kunwar, S., Roy, A., Bhusal, U., et al, 2023. Bio-fabrication of Cu/ Ag/Zn nanoparticles and their antioxidant and dye degradation activities[J]. Catalysts 13 (5), 891.

Lai, X., Ning, X., Chen, J., et al, 2020. Comparison of the Fe^{2+}/H$_2$O$_2$ and Fe^{2+}/PMS systems in simulated sludge: Removal of PAHs, migration of elements and formation of chlorination by-products [J]. J. Hazard. Mater. 398, 122826.

Li, X., Wang, N., Lv, G., et al, 2022. Experimental and theoretical insight into the transformation behaviors and risk assessment of Flutamide in UV/O3/PMS system[J]. J. Clean. Prod. 375, 134167.

Li, W., Zhang, H., Chen, P., et al, 2023. One-step hydrothermal deposition of Ag-doped g-C3N4-TiO2 nanocomposites on cotton fabric surface with enhanced photocatalytic activity[J]. Fibers Polym. 24 (2), 575–588.

Li, R., Zhou, C., Yang, L., et al, 2022. Multifunctional cotton with PANI-AgNPs heterojunction for solar-driven water evaporation[J]. J. Hazard. Mater. 424, 127367.

Liu, D., Chen, D., Hao, Z., et al, 2022. Efficient degradation of Rhodamine B in water by CoFe$_2$O$_4$/H$_2$O$_2$ and CoFe$_2$O$_4$/PMS systems: A comparative study[J]. Chemosphere 307, 135935.

Liu, Q., Xu, Q., Sun, W., 2021. Facile preparation of core-shell magnetic organic covalent framework via self-polymerization of two-in-one strategy as a magnetic solid-phase extraction adsorbent for determination of Rhodamine B in food samples[J]. J. Chromatogr. A 1657, 462566.

López, C., Valade, A.G., Combourieu, B., et al, 2004. Mechanism of enzymatic degradation of the azo dye Orange II determined by ex situ 1H nuclear magnetic resonance and electrospray ionization-ion trap mass spectrometry[J]. Anal. Biochem. 335 (1), 135–149.

Lu, C., Zhou, H., 2022. The Ag-based SPR effect drives effective degradation of organic pollutants by BiOCOOH/AgBr composites [J]. Adv. Powder Technol. 33, (3) 103428.

Mia, M.S., Yan, B., Zhu, X., et al, 2019. Dopamine grafted iron-loaded waste silk for Fenton-like removal of toxic water pollutants [J]. Polymers 11 (12), 2037.

Muthulakshmi, L., Rajini, N., Rajalu, A.V., et al, 2017. Synthesis and characterization of cellulose/silver nanocomposites from bioflocculant reducing agent[J]. Int. J. Biol. Macromol. 103, 1113–1120.

Nagar, N., Devra, V., 2019. Textile dyes degradation from activated peroxomonosulphate by green synthesize silver nanoparticles: a kinetic study[J]. J. Inorg. Organomet. Polym Mater. 29 (5), 1645–1657.

Patel, V.R., Bhatt, N.S., Bbhatt, H., 2013. Involvement of ligninolytic enzymes of Myceliophthora vellerea HQ871747 in decolorization and complete mineralization of Reactive Blue 220[J]. Chem. Eng. J. 233, 98–108.

Patil, S.B., Naik, H.S.B., Nagaraju, G., et al, 2018. Sugarcane juice mediated eco-friendly synthesis of visible light active zinc ferrite nanoparticles: application to degradation of mixed dyes and antibacterial activities[J]. Mater. Chem. Phys. 212, 351–362.

Rahn Kim, M., Seong, A.C., Shin, D., et al, 2008. Shape transformation and relaxation dynamics of photoexcited TiO$_2$/Ag nanocomposites[J]. J. Nanosci. Nanotechnol. 8 (6), 3197–3202.

Sabouri, Z., Sabouri, S., Tabrizi Hafez Moghaddas, S.S., et al, 2022. Facile green synthesis of Ag-doped ZnO/CaO nanocomposites with Caccinia macranthera seed extract and assessment of their cytotoxicity, antibacterial, and photocatalytic activity[J]. Bioprocess Biosyst. Eng. 45 (11), 1799–1809.

Saidin, S., Chevallier, P., Kadir, M.R.A., et al, 2013. Polydopamine as an intermediate layer for silver and hydroxyapatite immobilisation on metallic biomaterials surface[J]. Mater. Sci. Eng. C 33 (8), 4715–4724.

Tu, Y., Chen, J., Shao, G., et al, 2022. Preparation and application of green calcium-based catalyst for advanced treatment of salty wastewater with ozone[J]. J. Clean. Prod., 132464

Udomkun, P., Boonupara, T., Smith, S.M., et al, 2022. Green Ag/ AgCl as an effective plasmonic photocatalyst for degradation and mineralization of methylthioninium chloride[J]. Separations 9 (8), 191.

Wang, K., Dong, Y., Yan, Y., et al, 2017. Mussel-inspired chemistry for preparation of superhydrophobic surfaces on porous substrates [J]. RSC Adv. 7 (46), 29149–29158.

Wang, W., Jiang, Y., Wen, S., et al, 2012. Preparation and characterization of polystyrene/Ag core–shell microspheres–A bioinspired poly (dopamine) approach[J]. J. Colloid Interface Sci. 368 (1), 241–249.

Wang, X., Liu, X., Han, Q., et al, 2020. Photo-assisted Ag/AgCl nanoparticle formation process can be used in the degradation of fluorescent dyes[J]. Inorg. Chem. Commun. 112, 107716.

Wang, L., Ren, X., Chen, L., et al, 2023. Constructing recyclable photocatalytic BiOBr/Ag nanowires/cotton fabric for efficient dye degradation under visible light[J]. Arab. J. Chem. 16, (4) 104624.

Wang, Y., Wang, Q., Song, X., et al, 2019. Hydrophilic polyethylenimine modified magnetic graphene oxide composite as an efficient support for dextranase immobilization with improved stability and recyclable performance[J]. Biochem. Eng. J. 141, 163–172.

Xie, A., Wang, B., Chen, X., et al, 2021. Facile fabrication of superhydrophobic polyester fabric based on rapid oxidation polymerization of dopamine for oil–water separation[J]. RSC Adv. 11 (43), 26992–27002.

Xin, Z., Duan, K., Zhuo, Q., et al, 2023. Novel nanozyme Ag/ Fe3O4@ h-BN with peroxidase-mimicking and oxidase-mimicking

activities for dye degradation, As (V) removal and detection[J]. Chem. Eng. J. 461, 141589.

Xue, C.H., Ji, X.Q., Zhang, J., et al, 2015. Biomimetic superhydrophobic surfaces by combining mussel-inspired adhesion with lotus-inspired coating[J]. Nanotechnology 26, (33) 335602.

Y F, Wang Y J, Liao X. Degradation effect of phenol in simulated wastewater by CuO/Ac catalyzed persulfate[J]. Research of Environmental Sciences, 2018, 31(11): 1949-1956.

Zangmeister, R.A., Morris, T.A., Tarlov, M.J., 2013. Characterization of polydopamine thin films deposited at short times by autoxidation of dopamine[J]. Langmuir 29 (27), 8619–8628.

Zhang, Q., Huang, H., Fu, B., 2014. Construction and exploration of pollutant consumption oxygen equivalent treatment costs in municipal wastewater treatment plants[J]. Desalin. Water Treat. 52 (16–18), 3076–3084.

Zhang, N., Peng, S., Liu, Z., et al, 2022. AgNPs decorated on the magnetic $Fe_3O_4@$ PDA as efficient catalyst for organic pollutants removal and as effective antimicrobial agent for microbial inhibition[J]. J. Alloy. Compd. 928, 167257.

Zhang, D., Wei, E., Jing, H., et al, 2022. Facile construction of superhydrophobic polydopamine-based film and its impressive anti-corrosion performance on zinc surface[J]. Mater. Chem. Phys. 282, 125935.

Zhang, W., Yang, Z.Y., Cheng, X.W., et al, 2019. Adsorption, antibacterial and antioxidant properties of tannic acid on silk fiber [J]. Polymers 11 (6), 970.

Zhou, Q., Wu, W., Zhou, S., et al, 2020. Polydopamine-induced growth of mineralized γ-FeOOH nanorods for construction of silk fabric with excellent superhydrophobicity, flame retardancy and UV resistance[J]. Chem. Eng. J. 382, 122988.

Zhou, Y., Zhang, W., 2022. Nucleophilic modification of flavonoids for enhanced solubility and photostability towards uniform colouration, bio-activation and ultraviolet-proof finishing of silk fabric[J]. Arab. J. Chem. 15, (12) 104343.

Zimmermann, T., Kulla, H.G., Leisinger, T., 1982. Properties of purified Orange II azoreductase, the enzyme initiating azo dye degradation by Pseudomonas KF46[J]. Eur. J. Biochem. 129 (1), 197–203.